I&EC research
Industrial & Engineering Chemistry Research

Article

pubs.acs.org/IECR

Detection and Isolation of Batch-to-Batch Parametric Drift in Crystallization Using In-Batch and Post-Batch Measurements

Joseph Sang-Il Kwon,[†] Michael Nayhouse,[†] and Panagiotis D. Christofides*[,†,‡]

[†]Department of Chemical and Biomolecular Engineering, University of California, Los Angeles, California 90095, United States
[‡]Department of Electrical Engineering, University of California, Los Angeles, California 90095, United States

ABSTRACT: In this work, we focus on the development of a parametric drift detection and isolation (PDDI) method for the handling of batch-to-batch parametric drifts in a batch crystallization process used to produce hen egg-white (HEW) lysozyme crystals. We consider that the batch crystallization process is controlled by an in-batch model predictive control (MPC) system and is subject to batch-to-batch parametric drifts in the solubility, growth rates, continuous-phase mass and energy balance parameters, and nucleation rate. The proposed PDDI scheme consists of two parts: preparatory stage before batch-to-batch operation and post-batch stage during batch-to-batch operation. The goal of the preparatory stage is to compute the threshold values and signatures for each parametric drift using simulations and batch process common cause variance described by noise. During batch-to-batch operation, the proposed PDDI system monitors closed-loop process residuals, which are computed by taking the difference between the time profiles of the states obtained through in-batch and postbatch measurements from the time profiles of the states obtained from the drift-free simulation with noise. While the measurements of the protein solute concentration and the temperature in the crystallizer are available in real-time, post-batch measurements are usually available for the quality of the crystal products (e.g., number of crystals, average crystal size and shape) and this key characteristic is taken into account in the PDDI method. We then compare the residuals with signatures obtained in the preparatory stage for each parametric drift for isolation of a parametric drift. The PDDI system estimates the magnitude of the parametric drift and updates the parameters of the batch process model used in the in-batch MPC system to compute a set of jacket temperatures for the production of crystals with a desired shape distribution in the next batch. The performance of the MPC with the proposed PDDI scheme is demonstrated by applying it to a multiscale simulation of a batch crystallization process with parametric drifts in the solubility and crystal growth rates. The closed-loop system simulations demonstrate that crystals with a crystal shape distribution that is closer to a desired set-point value are produced under a parametric-drift handling scheme that integrates the in-batch MPC with the proposed PDDI system compared to those under the MPC with the nominal process model.

INTRODUCTION

Modeling and control of batch crystallization is of significant interest to the pharmaceutical industry, because the bioavailability of drugs is highly dependent on the size and shape distributions of their active pharmaceutical ingredients. Within this context, the dominant dynamic behavior of the evolution of key crystallization variables is modeled through a process model, which is used to compute a set of manipulated inputs that drives the average crystal shape to a desired setpoint at the end of the batch. However, because of unknown batch-to-batch parametric drifts, the process model employed for in-batch control and estimation purposes may significantly deviate from the actual process behavior. For example, a small batch-to-batch change in the pH level or impurity concentration in the feedstock container may significantly alter the quality (e.g., size and shape) of the crystal products.

Model-free control schemes, such as a proportional−integral−derivative (PID) control scheme, are not able to handle constraints on the inputs, outputs, and the rate of change of inputs while computing optimal jacket temperature values. Therefore, the necessity of incorporating the constraints to account for the physical limitations on the manipulated inputs and operating conditions makes model-based control strategy (e.g., refs 1−4) the method of choice for crystal size distribution control. More specifically, the model predictive control (MPC) scheme was employed in refs 5−8 in order to control the crystal size and shape distributions, along with the consideration of the crystal growth and nucleation processes in both batch and mixed suspension mixed product removal (MSMPR) processes, based on a reduced-order model.

With the ultimate goal of better understanding of the effect of variation in the process model parameters on the size and shape distributions of crystals produced by batch crystallization processes, this work considers the estimation of kinetic parameters when there exist batch-to-batch parametric drifts in multiple sources. A commonly used method to estimate process model parameters is the method of least-squares,[9,10] where its application to a crystallization process can be found in, for example, ref 11. In addition, the Bayesian approach has been applied to many chemical engineering problems, because of its capability to predict the occurrence of a parametric drift in the next batch run by taking into account historical batch process data.[12−15] Lastly, considering the repetitive nature of operation of a batch process, the general idea of the run-to-run (R2R) control scheme has been applied to address batch-to-

Received: January 30, 2015
Revised: April 9, 2015
Accepted: May 4, 2015
Published: May 4, 2015

DOI: 10.1021/acs.iecr.5b00422
Ind. Eng. Chem. Res. 2015, 54, 5514−5526

batch parametric drifts in a variety of batch processes.[16−20] In particular, when there is a noticeable trend in the batch-to-batch parametric drift, utilizing post-batch measurements over multiple batch runs through a moving horizon estimation (MHE) scheme guarantees the improved control performance from batch to batch.[21]

In the context of continuously improving batch process monitoring and control schemes, the design of systems capable of timely detection and isolation of batch-to-batch parametric drift and efficient handling of such drift has received growing attention. Generally, parametric drift detection and isolation (PDDI) methods can be divided into two categories: model-based and data-based.

Specifically, model-based PDDI schemes rely on mathematical models of the process developed from first-principles that can be solved in real time. With an accurate process model, the data generated from the batch process model are compared with process measurements to calculate residuals that will be used for the detection and isolation of a specific parametric drift in a manner similar to model-based fault detection and isolation.[22−24] On the other hand, data-based PDDI methods make use of process measurements in order to perform PDDI. Analyzing historical batch process data allows the construction of data-based thresholds for the residuals, which can be used to distinguish between normal and abnormal process operation.[25−27] A common characteristic of the aforementioned works on both model-based and data-based PDDI methods is that they only consider synchronously sampled measurements (e.g., real-time measurements in continuous processes), and they do not account for measurements that arrive asynchronously (e.g., post-batch measurements in batch processes). Motivated by these considerations, the goal of this work is to develop a PDDI scheme for a batch protein crystallization process where the protein solute concentration and the temperature in the crystallizer are available in real time (i.e., in-batch) at each sampling time, while only post-batch measurements are available for the number of crystals, average crystal size, and average crystal shape. This is due to the nature of the measurement techniques, because the measurements of crystal quality (such as the crystal size and shape distributions) are difficult to obtain in real time with high accuracy,[28,29] while real-time measurements of the solute concentration and of the temperature are usually available in the crystallizer.[30,31]

In a previous work of our group (cf. ref 21), we developed a R2R model parameter estimation scheme based on MHE concepts. This method brought together R2R control and optimization-based parameter estimation schemes. Provided that a nonlinear trend exists in the batch-to-batch parametric drift and it can be approximately modeled by an explicit function, it becomes possible to perform PDDI utilizing post-batch measurements from multiple batches, following a moving horizon approach. The purpose of the present work is to further refine the approach proposed in ref 21 by relaxing the requirement of the process measurements over multiple batch runs and developing the use of the proposed PDDI scheme for the detection and isolation of the parametric drift. Thus, it becomes easier to precisely calculate the magnitude of the process drift, because we determine the parameter(s) in which the parametric drift is located. First, a PDDI scheme is proposed for the purpose of the detection and isolation of parametric drifts introduced to a batch crystallization process. Then, a parametric drift-tolerant control scheme (PDTC) is proposed that uses the PDDI scheme to improve the model of the in-batch model predictive controller (MPC) to achieve the production of crystals with a desired shape distribution.

The manuscript is organized as follows: we initially describe a batch crystallization model used for our case study. Then, we develop the PDDI and in-batch MPC schemes in order to detect, isolate, and handle batch-to-batch parametric drifts. This is followed by the section of closed- loop simulation results, where the control and estimation performances of the proposed schemes to various batch-to-batch parametric drifts in the process model parameters are presented. For demonstration purposes, we consider two cases: parametric drifts in the growth rates and solubility curve. Lastly, the closed-loop performance of the PDTC with MPC is compared with that of the MPC based on the nominal batch process model.

BATCH CRYSTALLIZATION MODEL

We focus on a batch crystallization process used to produce hen egg-white (HEW) lysozyme crystals in order to demonstrate the proposed technique for parametric drift detection and isolation.

Crystal Nucleation. The nucleation rate, $B(\sigma)$, of lysozyme crystals is given below:[32]

$$B(\sigma) = \begin{cases} 0.041\sigma + 0.063 & \text{for } \sigma \geq 3.11 \\ 8.0 \times 10^{-8} \exp(4.725\sigma) & \text{for } \sigma < 3.11 \end{cases} \quad (1)$$

$B(\sigma)$ has units of cm^{-3} s^{-1}. The supersaturation level (σ) is computed through the logarithmic ratio between the solute concentration in the continuous phase C and the solubility s as follows:

$$\sigma = \ln\left(\frac{C}{s}\right) \quad (2)$$

where the solubility is calculated using the following equation:[33]

$$s(T) = 2.88 \times 10^{-4}T^3 - 1.65 \times 10^{-3}T^2 + 4.62 \times 10^{-2}T + 6.01 \times 10^{-1} \quad (3)$$

and T is the temperature in the crystallizer (in °C).

Crystal Growth. The growth rate equations of Table 1 are originally adopted from ref 34 and used to model the crystal growth through the kMC simulation.

Please note that the desorption and migration rates depend on the surface microconfiguration (i.e., they take into account the number of nearest neighbors i). The crystal growth rates obtained from the kMC simulations are calibrated with the experimental data[35] by manipulating a set of E_{pb} and ϕ values for the (110) and (101) faces and K_0^+ through extensive open-

Table 1. Surface Growth Rate Reactions[a]

surface reaction	rate equation
adsorption, r_a:	$K_0^+ \exp(\sigma)$
desorption, $r_d(i)$:	$K_0^+ \exp\left(\frac{\phi}{k_BT} - i\frac{E_{pb}}{k_BT}\right)$
migration $r_m(i)$:	$K_0^+ \exp\left(\frac{\phi}{k_BT} - i\frac{E_{pb}}{k_BT} + \frac{E_{pb}}{2k_BT}\right)$

[a] K_0^+ is the adsorption coefficient, ϕ is the total binding energy of a fully occupied lattice, i is the number of nearest neighbors, and E_{pb} is the average bonding energy per bond.

DOI: 10.1021/acs.iecr.5b00422
Ind. Eng. Chem. Res. 2015, 54, 5514−5526

loop kMC simulations. The parameters used for the kMC simulation are listed in Table 2. The reader may refer to ref 36 for more details regarding the execution of the kMC simulation.

Table 2. Parameters for the Faces (110) and (101) at 4% (w/v) NaCl and pH = 4.5 at T = 18 °C[a]

	Value	
parameter	(110) face	(101) face
E_{pb}/k_B	1077.26	800.66
ϕ/k_B	227.10	241.65

[a] $K_0^+ = 0.211\ s^{-1}$.

Mass and Energy Balance Equations. The following mass and energy balance equations[37] are employed in this work to compute the evolution of the solute concentration and temperature in the crystallizer with time:

$$\frac{dC}{dt} = -\frac{\rho_c}{V_{batch}}\frac{dV_{crystal}}{dt}, \quad C(0) = 48\ mg/cm^3 \tag{4}$$

$$\frac{dT}{dt} = -\frac{\rho_c \Delta H_c}{\rho C_p V_{batch}}\frac{dV_{crystal}}{dt} - \frac{U_c A_c}{\rho C_p V_{batch}}(T - T_j), \quad T(0) = 17°C \tag{5}$$

where $V_{crystal}$ is the total volume of crystals in the crystallizer and T_j is the jacket temperature (i.e., manipulated input). The process parameter values are shown in Table 3.

Table 3. Parameters for the Batch Crystallizer Model

symbol	property	value
ρ_c	crystal density (mg/cm^3)	1400
ΔH_c	enthalpy of crystallization (kJ/kg)	−4.5
$\rho(t)$	density of the continuous phase (mg/cm^3)	1000 + $C(t)$
C_p	specific heat capacity (kJ/(K kg))	4.13
V_{batch}	volume of the crystallizer (L)	1
A_c	contact area of the crystallizer wall and jacket (m^2)	0.25
U_c	overall heat transfer coefficient (kJ/(m^2 h K))	1800

The enthalpy of crystallization is taken from ref 38, and the specific heat capacity of the solution is assumed to be identical to that of water, since the amount of the protein solute in the solution is small, in comparison to that of water.

While it would be difficult to capture in the crystallizer model, in which the control action is applied to, the entire plant physical realization, the model employed here accounts for a significant part of the complexity of a crystallization process, including its multiscale character.

Population Balance Equation. The evolution of the crystal volume distribution for the batch crystallization process with nucleation and crystal growth is described by the following population balance equation (PBE):[39]

$$\frac{\partial n(V,t)}{\partial t} + \frac{\partial (G_{vol}(V,\sigma)n(V,t))}{\partial V} = B\delta(V) \tag{6}$$

where $n(V,t)$ is the number of crystals of volume V at time t, $\delta(\cdot)$ is the dirac delta function, and $G_{vol}(V,\sigma)$ is the volumetric crystal growth rate which will be formulated with more details in the following section. Equation 6 states that crystals are nucleated with an infinitesimal size. The dirac function in the population balance equation capturing the effect of nucleation rate will be stated as a boundary condition and used to simulate the nucleation process.

Moment Models. By applying the method of moments to the PBE of eq 6, a moments model that describes the zero and first moments of the crystal volume distribution in the batch crystallizer can be derived using standard techniques and has the following form:[37]

$$\frac{dM_0}{dt} = B \tag{7}$$

$$\frac{dM_1}{dt} = G_{vol}M_0 \tag{8}$$

where $M_j(t) = \int_0^\infty V^j n(V,t)\,dV$ is the jth moment for j = 0, 1, and G_{vol} is formulated as follows:

$$G_{vol} = 2G_{110}\langle h_{110}\rangle\langle h_{101}\rangle + G_{101}\langle h_{110}\rangle^2 \tag{9}$$

where G_{110} and G_{101} are the crystal growth rates in the direction of the (110) and (101) faces (cf. Figure 1), respectively. The following polynomial expressions for the growth rates G_{110} and G_{101} are obtained from open-loop simulations of the multiscale model used to model the batch crystallization process:

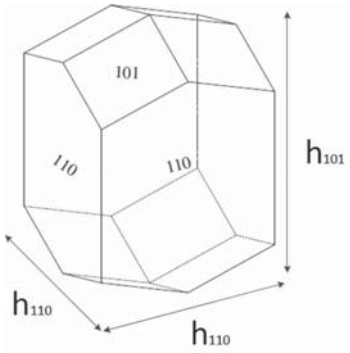

Figure 1. HEW lysozyme crystal.

$$G_{110} = 0.1843\sigma^3 - 1.1699\sigma^2 + 2.8885\sigma - 2.5616 \tag{10}$$

and

$$G_{110} = 0.1893\sigma^3 - 1.2264\sigma^2 + 2.9887\sigma - 2.5348 \tag{11}$$

Lastly, the dynamic evolution of the average crystal heights, $\langle h_{110}\rangle$ and $\langle h_{101}\rangle$, are formulated as follows:

$$\frac{d\langle h_{110}\rangle}{dt} = G_{110} - \frac{BV_{batch}\langle h_{110}\rangle}{M_0}$$

$$\frac{d\langle h_{101}\rangle}{dt} = G_{101} - \frac{BV_{batch}\langle h_{101}\rangle}{M_0} \tag{12}$$

Thus, the average crystal shape, $\langle\alpha\rangle$, and size, $\langle V\rangle$, can be computed as follows:

$$\langle\alpha\rangle \approx \frac{\langle h_{110}\rangle}{\langle h_{101}\rangle} \quad \langle V\rangle = \frac{M_1}{M_0} \tag{13}$$

The reader may refer to ref 40 for a more-detailed derivation of the moments model.

DOI: 10.1021/acs.iecr.5b00422
Ind. Eng. Chem. Res. 2015, 54, 5514−5526

PARAMETRIC DRIFT DETECTION AND ISOLATION SYSTEM DESIGN

In-Batch MPC. We initially design an in-batch model predictive controller (MPC) for the drift-free batch crystallization process used for the production of HEW lysozyme crystals. First, the dominant dynamic behavior of the evolution of the crystal shape distribution in the batch crystallization process is modeled through the process model (cf. eqs 1−13), which is used to compute a set of optimal jacket temperatures that minimizes the squared deviation of the average crystal shape from a target value over the entire prediction horizon. We note that the term "optimal" is used for constrained optimization as well, in reference to a solution that optimizes the cost functions while satisfying the constraints. There are constraints imposed on the rate of change of the jacket temperature and on the magnitude of the temperature in the crystallizer. The resulting optimization problem for the proposed in-batch MPC is formulated as follows:

$$\min_{T_{j,1},\ldots,T_{j,p}} \sum_{i=1}^{p} \left(\langle\alpha(t_i)\rangle - \alpha_{set}\right)^2 \tag{14a}$$

$$\text{s.t. eqs } 1-13 \tag{14b}$$

$$4^\circ\text{C} \le T \le 25^\circ\text{C} \qquad \left|\frac{T_{j,i+1} - T_{j,i}}{\Delta}\right| \le 2\ ^\circ\text{C/min} \tag{14c}$$

$$t_i = t + i\Delta \tag{14d}$$

where p is the length of the prediction horizon ($p = 10$), Δ the sampling time ($\Delta = 40$ s), and $T_{j,i}$ the jacket temperature at the ith prediction step t_i. The *in situ* measurements of C and T are available at every sampling instant. Then, the optimization problem of eqs 14 is solved to compute a set of optimal jacket temperatures, ($T_{j,1}$, ..., $T_{j,10}$), and the first value, $T_{j,1}$, is applied to the crystallizer until the next sampling instant. Note that, since we impose explicit constraints on the magnitude of the crystallizer temperature, there is no need to impose explicit constraints of the magnitude of the jacket temperature (i.e., manipulated input), because it is implicitly constrained by the crystallizer temperature constraint. The simulations were carried out on the Hoffman2 cluster at UCLA and the optimization problems were solved using the open source interior point optimizer, IPOPT.

Parametric Drift Detection and Isolation. We consider batch-to-batch parametric drifts in a batch crystallization process, particularly in the parameters of the mass and energy balance equations, the nucleation and crystal growth rate expressions, and the solubility expression. These batch-to-batch parametric drifts can be detected and isolated by observing the evolution of measured outputs of the closed-loop system through in-batch (e.g., C, T) and post-batch (e.g., $\langle\alpha\rangle$, M_0, $\langle h_{110}\rangle$, $\langle h_{101}\rangle$) measurement techniques. This consideration requires that each parametric drift be the one influencing a certain subset of the process outputs (i.e., each parametric drift has a unique parametric drift signature).

As described in Figure 2, we first design and employ a PDDI scheme in order to detect a parametric drift in real time over the course of a batch run via in-batch measurements and to further detect the drift at the end of a batch run via post-batch measurements. The information generated by the nominal batch crystallizer model initialized at the same state as the actual batch process, provides an estimate of the parametric

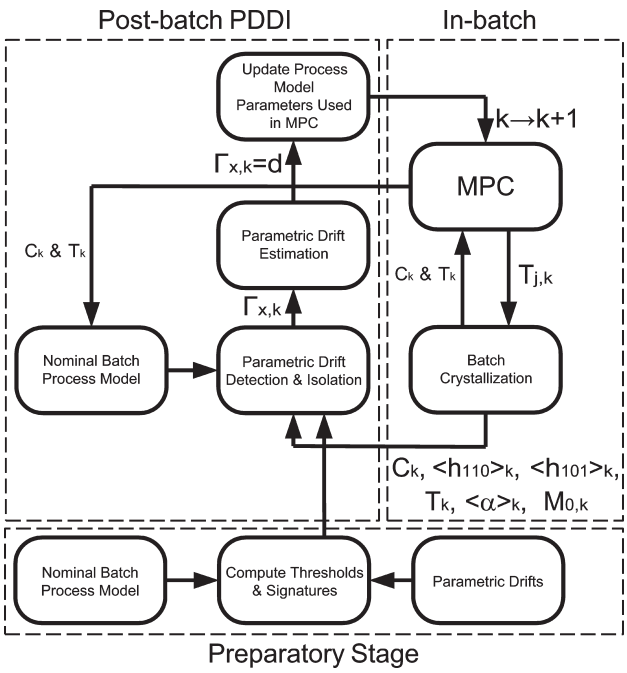

Figure 2. Structure integrating parametric-drift detection and isolation scheme with in-batch MPC.

drift-free batch process variables and allows detection of the parametric drifts by comparing the nominal behavior with the actual process behavior (i.e., in-batch and postbatch process measurements). Specifically, the PDDI residual for each variable can be defined as

$$r_x(t) = |\bar{x}(t) - x(t)| \quad \text{for } x \in \{C, T\}$$
$$r_x(t_f) = |\bar{x}(t_f) - x(t_f)| \quad \text{for } x \in \{\langle\alpha\rangle, M_0, \langle h_{110}\rangle, \langle h_{101}\rangle\} \tag{15}$$

where $\bar{x}$ is the predicted evolution for the variable x, which is obtained from the nominal process model (cf. eqs 1−13) with noise for the same initial state and input trajectory as the one applied to the actual batch process. The residuals r_T and r_C are calculated at every sampling instant through in-batch measurements while residuals $r_{\langle\alpha\rangle}$, r_{M_0}, $r_{\langle h_{110}\rangle}$, and $r_{\langle h_{101}\rangle}$ are evaluated once, using the above procedure at the end of the batch run, because only post-batch measurements are available for those variables.

When there is a parametric drift in the process from batch-to-batch, process residuals affected directly by the parametric drift will deviate from zero. Furthermore, it is assumed that the parametric drifts of interest will be sufficiently large so that their effect will not be masked by process or measurement noise. Therefore, the thresholds, with respect to which the residuals will be compared, should account for the effect of process and measurements noise. If no parametric drift occurs, the measurements are close to the nominal behavior (depending on the process and measurement noises levels) obtained via post-batch closed-loop kMC simulations, using the input profile applied to the process at the last batch run. However, because of process and sensor measurement noise, the residuals $r_x(t)$ will be nonzero. This necessitates the use of parametric drift detection thresholds so that a parametric drift in the variable x is declared only when a residual exceeds a specific threshold value, $r_{x,max}$, that accounts explicitly for the effect of process and

DOI: 10.1021/acs.iecr.5b00422
Ind. Eng. Chem. Res. 2015, 54, 5514−5526

measurement noise. Below, we describe the PDDI scheme in detail.

Specifically, the proposed PDDI scheme consists of two parts: preparatory stage before batch-to-batch operation and post-batch stage during batch-to-batch operation. Before batch-to-batch operations, the goal of the preparatory stage is to compute the threshold values and signatures for each parametric drift and it is described as follows:

(1) In the preparatory stage, we simulate batch runs under the MPC with the nominal process model. The noise (common cause variance), which is obtained from historical data and sensor information, is added to the process model used to simulate the batch crystallization process but not added to the batch process model used in the MPC. Then, these runs are used along with the same type of simulations for batch runs under MPC but without noise to compute residuals and calculate the threshold value for each variable x ($r_{x,\max}$), based on the maximum deviation (absolute values) of the time profiles of the residuals with and without noise from zero (difference of the time profiles of the variables of these two distinct sets of simulations), respectively.

(2) We also calculate signatures for each drift in the preparatory stage. We simulate batch runs under MPC with the nominal process model. Again, the noise is added to the process model used to simulate batch crystallization, but it is not added to the process model used in the MPC. Furthermore, we add a parametric drift in each of the five variables separately (i.e, therefore we need at least as many separate simulations as the number of drifts considered). We then compute the residuals for each variable by calculating the difference between the time profiles of the states obtained using this simulation with parametric drifts and the time profiles of the variables obtained from the simulation, where it has noise but no drift in the process model. The residual of C and T that exceeds its threshold first is recorded, and the signature of this specific drift is calculated.

Note that if two or more parametric drifts are defined by the same signature, isolation between them is not possible on the basis of the parametric drift signature (i.e., no isolation). This problem will be addressed via another set of simulations discussed below. The post-batch stage of the proposed PDDI scheme during batch-to-batch operation is described as follows:

(1) At the end of each batch run, we compute the residuals by calculating the difference between the time profiles of the states obtained through in-batch and post-batch measurements from the time profiles of the states obtained from the drift-free simulation with noise using the input trajectory applied to the process during the last batch. Then, we compare these residuals (calculated post-batch) with signatures obtained in the preparatory stage for each parametric drift.

(2) After we narrow down the overall set of drift candidates to a few parametric drift candidates, we run optimization problems with the remaining drift candidates to match simulated drift behavior with the in-batch experimental output post-batch measurements in order to isolate the parametric drift and to estimate the magnitude of the parametric drift. Details of this step are given below in the Parametric Drift Estimation section.

(3) The parameters of the batch process model used in the MPC for the next batch then is updated to account for the presence of drift.

Precise isolation of the parametric drift, such as the one attained by the proposed PDDI scheme, would allow for the design of a model predictive controller that will directly handle the parametric drift in its formulation by updating its model before each batch. As a result, the PDDI scheme can enhance the controller performance by minimizing the production of crystals with undesired characteristics attributed to the parametric drift.

Also, it is important to point out the difference of the proposed PDDI scheme with the MHE formulation employed in ref 13 for computing parameter updates for the model used in the MPC in the next batch run. If the detection and isolation of the parametric drift is possible, then the model parameters that are being updated are only the ones that are being directly affected by the drift; as a result, the accuracy of the model used in the MPC in the next batch is superior to that of the model that uses a generic update for a larger set of its parameters.

Parametric Drift Estimation. After a parametric drift has been detected and isolated, the PDDI system will estimate the magni- tude of the parametric drift (i.e., how much the batch process is perturbed from a nominal batch behavior). If two or more parametric drifts are defined by the same signature, isolation between them is not possible on the basis of the parametric drift signature and, thus, we must find one drift that better matches the in-batch and the post-batch measurements by running the following optimization problem with candidates which have been narrowed down from the set of all possible drift candidates.

Specifically, a least-squares optimization problem is solved to estimate the magnitude of the particular parametric drift (one at a time) utilizing the in-batch and post-batch measurements (e.g., C, T, $\langle\alpha\rangle$, M_0, $\langle h_{110}\rangle$, $\langle h_{101}\rangle$) and the control inputs (e.g., T_j) applied in the last batch run. In the optimization problem of eqs 16 below, parametric drifts associated with the nucleation rate, the crystal growth rate in the direction of the (110) and (101) faces, the parameters of the solubility equation, and the parameters of the mass and energy balance equations are taken into account by multiplying the correction parameters γ_{nu}, γ_{110}, γ_{101}, γ_s, γ_C, and γ_T to the nominal expressions, respectively. Furthermore, the objective function (cf. eq 16a) consists of a sum of squared errors between the predicted average crystal size and shape, $\widehat{\langle\alpha(t_f)\rangle}$ and $\widehat{\langle V(t_f)\rangle}$, and the measured ones, $\langle\alpha\rangle_{\text{measured}}$ and $\langle V\rangle_{\text{measured}}$. The resulting optimization is formulated as follows:

$$\min_{\Gamma} w_\alpha(\widehat{\langle\alpha(t_f)\rangle} - \langle\alpha\rangle_{\text{measured}})^2 + w_V(\widehat{\langle V(t_f)\rangle} - \langle V\rangle_{\text{measured}})^2 \tag{16a}$$

$$\text{s.t. eqs } 1-14 \tag{16b}$$

$$\hat{s}(t) = \gamma_s s(t), \qquad \hat{B}(\sigma) = \gamma_{\text{nu}} B(\sigma) \tag{16c}$$

$$\hat{G}_{110}(t) = \gamma_{110} G_{110}(t), \qquad \hat{G}_{101}(t) = \gamma_{101} G_{101}(t) \tag{16d}$$

$$\hat{T}(t) = \gamma_T T(t), \qquad \hat{C}(t) = \gamma_C C(t) \tag{16e}$$

$$\Gamma = [\gamma_{110}, \gamma_{101}, \gamma_T, \gamma_C, \gamma_{\text{nu}}, \gamma_s] \tag{16f}$$

Assuming we have already isolated a parametric drift, we can use only one correction factor (cf. PDDI with γ_x) and leave the other entries equal to one. For example, if a parametric drift in the solubility equation has been isolated, the correction parameters in Γ become $\gamma_{110} = \gamma_{101} = \gamma_T = \gamma_C = \gamma_{\text{nu}} = 1$ and $\gamma_s = d$, where d is the magnitude of the parametric drift for the solubility equation. Therefore, solving the optimization

DOI: 10.1021/acs.iecr.5b00422
Ind. Eng. Chem. Res. 2015, 54, 5514−5526

problem of eqs 16 is reduced to finding the value of the magnitude d. If two or more parametric drifts are defined by the same signature, we have to run them one by one, as described above, until we find one that better matches the in-batch and post-batch measurements. Once the parametric drift is isolated and its magnitude d is estimated, the PDDI system will send the parametric drift information to the in-batch MPC to update its model, which will be used for the computation of the optimal jacket temperature in the next batch run. This control scheme is essentially a PDTC. A schematic representation of the PDTC scheme is shown in Figure 2.

Using the PDTC scheme, the parameters in the process model used in the MPC in the next batch are updated based on the parametric drift detection and isolation via the proposed PDDI scheme. The parametric drifts in the growth rates and the solubility curve are used for demonstration purposes. The proposed scheme can be applied to handle parametric drifts in the other parameters as well. However, the performance of the proposed PDDI scheme is dependent on the specific crystallization system, and in some cases, the parametric drift may be such that it is not possible to achieve good parametric drift detection and isolation.

While the decision variables in the optimization problems of eqs 14 (MPC) and 16 (post-batch parameter estimation) are finite, because of the sample-and-hold implementation of the control actions (jacket temperature) to the crystallizer and the estimation of a finite number of parameter values, respectively, the dynamics of the crystallizer taken into account in the MPC model are continuous, and, therefore, they are modeled by differential equations. Of course, these differential equations are integrated numerically with a much smaller time step than the sampling time during the solution of the MPC optimization problem at each sampling time that leads to the calculation of the control actions.

More specifically, the optimization problem of eq 14 was solved to local optimality using the open-source interior point optimizer, IPOPT, and the optimization problem of eq 16 was also solved to local optimality using the Matlab function *fmincon* at the end of the batch process. Although a negligible amount of time is needed for the former problem to be solved (well-within the sampling time limits), ∼5−10 s are needed for the latter.

APPLICATION OF MPC WITH PDDI TO BATCH PROTEIN CRYSTALLIZATION

Process and Measurement Noise. Measurement and process noise is added to the process model used to simulate the batch crystallization process. Specifically, measurement noise is introduced to the $C(t)$ and $T(t)$ measurements as follows:

$$C(t) = \bar{C}(t) + w_C(t), \qquad T(t) = \bar{T}(t) + w_T(t) \tag{17}$$

where $\bar{C}(t)$ and $\bar{T}(t)$ are the average solute concentration in the continuous phase and the crystallizer temperature, $w_C(t)$ and $w_T(t)$ are both Gaussian white noise with zero mean and a standard deviation of 2% of $\bar{C}(t)$ and $\bar{T}(t)$, respectively. Furthermore, the process noise is introduced to the nucleation and growth rates in the direction of the (110) and (101) faces as follows:

$$\begin{aligned} B(\sigma) &= \bar{B}(\sigma) + w_B(\sigma), \\ G_{110}(t) &= \bar{G}_{110}(t) + w_{G_{110}}(t), \\ G_{101}(t) &= \bar{G}_{110}(t) + w_{G_{110}}(t) \end{aligned} \tag{18}$$

where $\bar{B}(\sigma)$, $\bar{G}_{110}(t)$, and $\bar{G}_{101}(t)$ are the nominal nucleation rate and the growth rates in the direction of the (110) and (101) faces, $w_{B(\sigma)}$, $w_{G_{110}(t)}$, and $w_{G_{101}(t)}$ are also Gaussian white noise variables with zero mean and a standard deviation of 2% of $\bar{B}(\sigma)$, $\bar{G}_{110}(t)$, and $\bar{G}_{101}(t)$, respectively.

Drift-Free Operation and Parametric Drifts. In the Parametric Drift Estimation section, an in-batch MPC is designed for the drift-free batch crystallization process. The performance of the in-batch MPC is demonstrated by applying it to a drift-free closed-loop simulation with the noise under nominal operation conditions where Figure 3 shows the trajectory of the real-time in-batch measurements of $T(t)$ and $C(t)$ and Table 4 shows the post-batch measurements $\langle \alpha(t) \rangle$, $M_0(t)$, $\langle h_{110}(t) \rangle$, and $\langle h_{101}(t) \rangle$ at t = 18 h.

Note that, under drift-free operating conditions, the production of crystals with a shape distribution that is very close to a desired set-point value, α_{set} = 0.89, is achieved. The parametric drifts considered in this work and their magnitudes are given in Table 5. Specifically, the values corresponding to

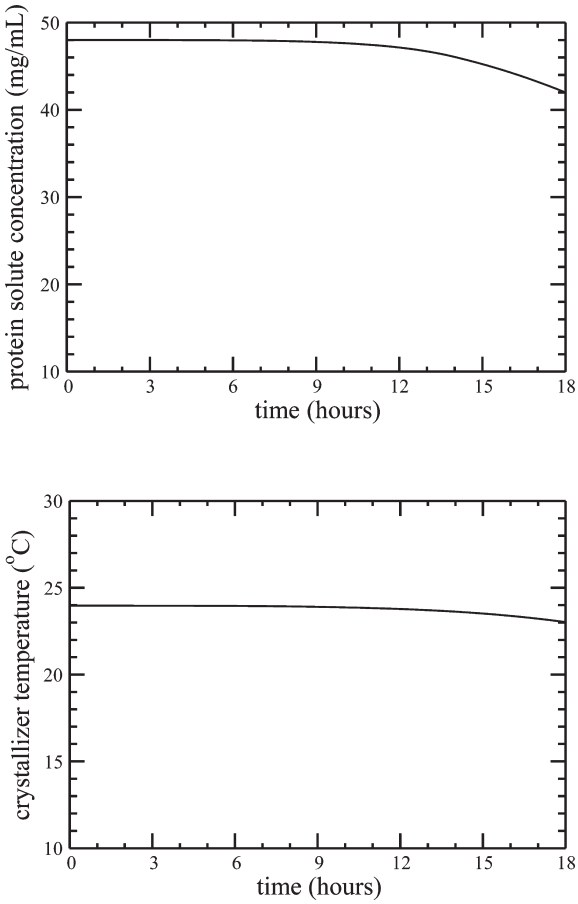

Figure 3. Profiles of the protein solute concentration and of the crystallizer temperature with time during batch crystallization under nominal (drift-free) operating conditions, for the growth rate ratio set-point value, α_{set} = 0.89.

DOI: 10.1021/acs.iecr.5b00422
Ind. Eng. Chem. Res. 2015, 54, 5514−5526

Table 4. Post-Batch Measurements for the Batch Crystallization Process under Drift-Free Closed-Loop Operation at t = 18 h

parameter	value
$\langle\alpha\rangle$	0.895
M_0	384 000
$\langle h_{110}\rangle$	174 μm
$\langle h_{101}\rangle$	185 μm

Table 5. Magnitude of Parametric Drift for Each Variable

type	% change of nominal value
ρ_c in mass balance, eq 4	−10%
U_c in energy balance, eq 5	−10%
G_{110} rate, eq 10	−30%
G_{101} rate, eq 11	−23%
nucleation rate, eq 1	+40%
solubility, eq 3	+10%

the percentage change presented in Table 5 for each variable are multiplied to the expressions for B, G_{110}, G_{101}, and S, respectively (e.g., multiply eq 10 by 0.7 to model the parametric drift described in Table 5 for G_{110}).

Preparatory Stage of PDDI. In the preparatory stage, we simulate batch runs using the process model with the noise under the MPC with the nominal process model. These runs then are used along with the same type of simulations for batch runs but without noise to get the threshold values that are mainly attributed to the effect of the noise in the process model. Specifically, the maximum value of each variable throughout the batch run is chosen as the threshold value for each variable ($r_{x,\max}$), and they are presented as follows:

$$r_{C,\max} = 1.4\,\mathrm{mg/cm^3}$$
$$r_{T,\max} = 1.1\,^\circ\mathrm{C}$$
$$r_{\langle\alpha\rangle,\max} = 0.021$$
$$r_{M_0,\max} = 64\,000$$
$$r_{\langle h_{110}\rangle,\max} = r_{\langle h_{101}\rangle,\max} = 10\,\mu\mathrm{m} \tag{19}$$

and signatures for each parametric drift are also determined based on these threshold values. First, in-batch measurements are used for detection and isolation of parametric drifts at the end of the batch. Specifically, a parametric drift is detected if $r_x(t_x) > r_{x,\max}$ for $x \in \{C, T\}$ where t_x is the first time r_x exceeds the threshold value $r_{x,\max}$. Depending on which residual exceeds its threshold first between C and T, the process signature for a parametric drift in the variable x, $W^{x,\mathrm{in}} = [W_C;W_T]$, is built as follows:

$$t_C > t_T \;\rightarrow\; [W_C;\, W_T] = [1;\, 0] \tag{20a}$$

$$t_C < t_T \;\rightarrow\; [W_C;\, W_T] = [0;\, 1] \tag{20b}$$

where, as a result, the possible candidates for parametric drifts can be divided into two subgroups based on their in-batch process signatures, $W^{x,\mathrm{in}}$, as follows:

$$W^{C,\mathrm{in}} = W^{S,\mathrm{in}} = W^{N,\mathrm{in}} = [1;\, 0]$$
$$W^{T,\mathrm{in}} = W^{G_{110},\mathrm{in}} = W^{G_{101},\mathrm{in}} = [0;\, 1] \tag{21}$$

If $t_C = t_T$, it indicates that the in-batch measurements are not able to be used for the isolation of parametric drifts. The post-batch measurements (e.g., $\langle\alpha\rangle$, M_0, $\langle h_{110}\rangle$, $\langle h_{101}\rangle$) then are used to compute the post-batch signature for a parametric drift in the variable x, $W_{x,\mathrm{post}} = [W_{\langle\alpha\rangle}, W_{M_0}, W_{\langle h_{110}\rangle}\ W_{\langle h_{101}\rangle}]$, as described below:

$$r_x > r_{x,\max} \;\rightarrow\; W_x = 1 \tag{22a}$$

$$r_x \le r_{x,\max} \;\rightarrow\; W_x = 0 \tag{22b}$$

for $x \in \{\langle\alpha\rangle,M_0,\langle h_{110}\rangle,\langle h_{101}\rangle\}$. Note that which one exceeds its threshold value first does not matter, because all residuals exceed their thresholds at t = 18 h. For example, if we simulate a batch run with a parametric drift in the solubility curve and observe that $r_x > r_{x,\max}$ for $\langle\alpha\rangle$, $\langle h_{110}\rangle$, and $\langle h_{101}\rangle$ only, we obtain the post-batch process signature for the parametric drift in the solubility curve, $W^{S,\mathrm{post}} = [1;0;1;1]$. In this work, however, all residuals will eventually exceed their thresholds and thus all signatures are identical as follows:

$$W^{C,\mathrm{post}} = W^{S,\mathrm{post}} = W^{N,\mathrm{post}} = W^{T,\mathrm{post}} = W^{G_{110},\mathrm{post}} = W^{G_{101},\mathrm{post}} = [1;1;1;1] \tag{23}$$

Therefore, it is not possible to further isolate parametric drifts based on the post-batch measurements (i.e., the post-batch measurements do not give any information for isolation of parametric drifts). Instead, once we have narrowed down to two subgroups using the in-batch measurements (cf. eq 21), we will run simulation for the remaining drift candidates one by one to find the one that better matches the in-batch and post-batch measurements.

Post-Batch Stage of PDDI. In the post-batch stage of the proposed PDDI, we compute the residuals by calculating the difference between the time profiles of the states obtained through in-batch and post-batch measurements from the time profiles of the states obtained from the drift-free simulation with noise used in the preparatory stage above. We then compare the residuals with signatures obtained in the preparatory stage for each parametric drift. An optimization problem then is solved to isolate the parametric drift and to estimate the magnitude of the parametric drift. Then, the batch process model used in the MPC for the next batch is updated.

Parametric Drift in Solubility. The first scenario considered in this work has a parametric drift triggered in the solubility equation producing crystals that do not meet the desired product quality. Specifically, a parametric drift (for example, a change in the pH level of a feedstock container) is introduced at the beginning of the batch run, such that the solubility is increased by 10% for a given temperature level. As a result, a set of the optimal jacket temperatures computed by the in-batch MPC using a nominal process model will not drive the temperature in the crystallizer to a desired level, because of the mismatch between the actual batch process and the solubility model used in the in-batch MPC.

We now look at how the PDDI system responds to the same parametric drift in the solubility equation. During batch-to-batch operations, the PDDI system performs two actions. First, at the end of each batch, it computes the residuals r_C and r_T, using in-batch measurements of those variables. If the residuals exceed their thresholds, a parametric drift is detected and isolated by comparing its in-batch process signature with the parametric drift signatures presented in eq 21. Specifically, the detection of a parametric drift is most evident in Figure 4 and

DOI: 10.1021/acs.iecr.5b00422
Ind. Eng. Chem. Res. 2015, 54, 5514−5526

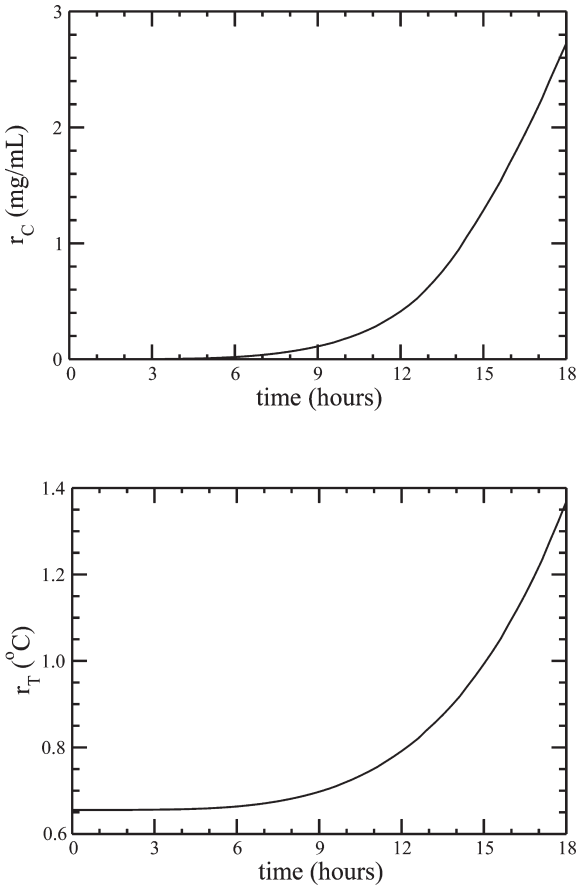

Figure 4. Residual profiles of the protein solute concentration (r_C) and of the crystallizer temperature (r_T) with time during batch crystallization, in response to a parametric drift in the solubility equation (eq 3), under the MPC scheme with the nominal process model, for a growth rate ratio set-point value of α_{set} = 0.89.

Table 6. Residuals Based on the Post-Batch Measurements Obtained at t = 18 h for the Batch Crystallization Process with a Parametric Drift in the Solubility Equation under No PDTC

parameter	value
$r_{\langle\alpha\rangle}$	0.17
r_{M_0}	128 000
$r_{\langle h_{110}\rangle}$	40.1 μm
$r_{\langle h_{101}\rangle}$	34.8 μm

Table 6, where the residuals $r_C(t)$ and $r_T(t)$ exceed their thresholds at t = 15.2 and t = 16 h, while $r_{\langle\alpha\rangle}(t)$, $r_{M_0}(t)$, $r_{\langle h_{110}\rangle}(t)$, and $r_{\langle h_{101}\rangle}(t)$ exceed their threshold values at t = 18 h. The resulting in batch process signature [1;0] coincides with the signatures for parametric drifts in the solubility curve, mass balance parameters, or nucleation rate (cf. eq 21). Since, in this work, the post-batch measurements do not provide any information for isolation of the parameter drift, the second action of the PDDI scheme is to determine the one that better matches the in-batch and post-batch measurements. Assuming that only one parametric drift occurs at a single batch, the magnitude of each parametric drift is computed by solving eqs 16 for γ_s, γ_C, and γ_{nu} separately. As a result, the correction parameter for the solubility equation gives the best matching with the process measurements when γ_s = +10%. This information is used to update the model of the MPC system to deal with the persistent parametric drift in the solubility curve that would have an effect on the product quality in the next batch run. The performance of the successful model parameter updating at the next batch run can be seen in Figure 5 and Table 7, where the residuals obtained by the multiscale simulations under the PDTC scheme remain far below their threshold values.

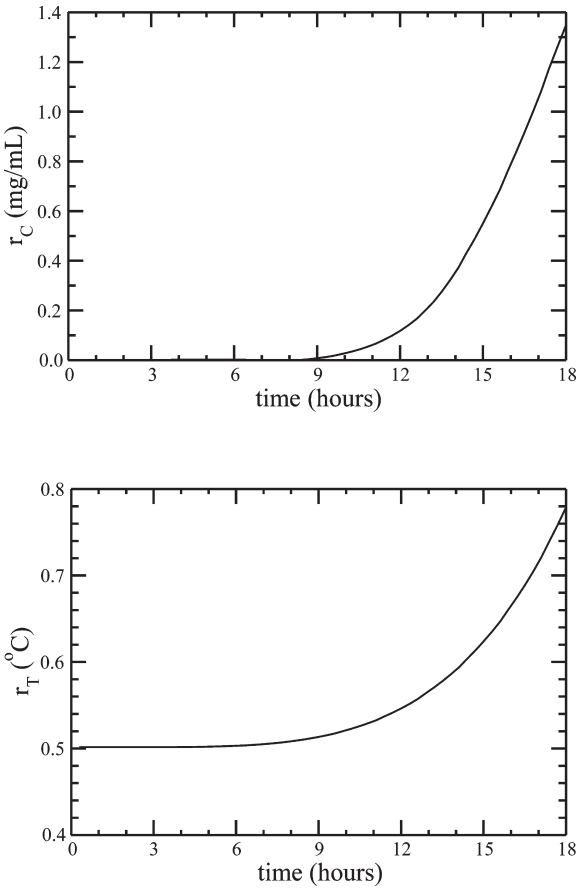

Figure 5. Residual profiles of the protein solute concentration (r_C) and of the crystallizer temperature (r_T), relative to time during batch crystallization, in response to a parametric drift in the solubility equation (eq 3), under the PDTC scheme with γ_s, for a growth rate ratio set-point value of α_{set} = 0.89.

For the purpose of testing of the closed-loop performance, with respect to the use of more correction factors, the control performance of the PDTC with γ_s is compared with that of the PDTC with Γ, where all six correction factors are used to compensate for the parametric drift in the solubility equation. In Figure 6 and Table 7, the residuals obtained under the PDTC with γ_s are smaller than those under the PDTC with Γ, indicating that the former scheme estimates the effect of the process drift in the solubility curve better than the latter scheme. It is also apparent in Figure 7 that the crystal shape distribution obtained at t = 18 h under the PDTC with γ_s is

DOI: 10.1021/acs.iecr.5b00422
Ind. Eng. Chem. Res. 2015, 54, 5514−5526

Table 7. Comparison of the Residuals Based on the Post-Batch Measurements for the Batch Crystallization Process with a Parametric Drift in the Solubility Equation under PDTC Scheme with γ_s and PDTC Scheme with Γ at t = 18 h

	Value	
parameter	PDTC with γ_s	PDTC with Γ
$r_{\langle\alpha\rangle}$	0.0047	0.019
r_{M_0}	32000	92000
$r_{\langle h_{110}\rangle}$	1.95 μm	12.1 μm
$r_{\langle h_{101}\rangle}$	1.72 μm	8.51 μm

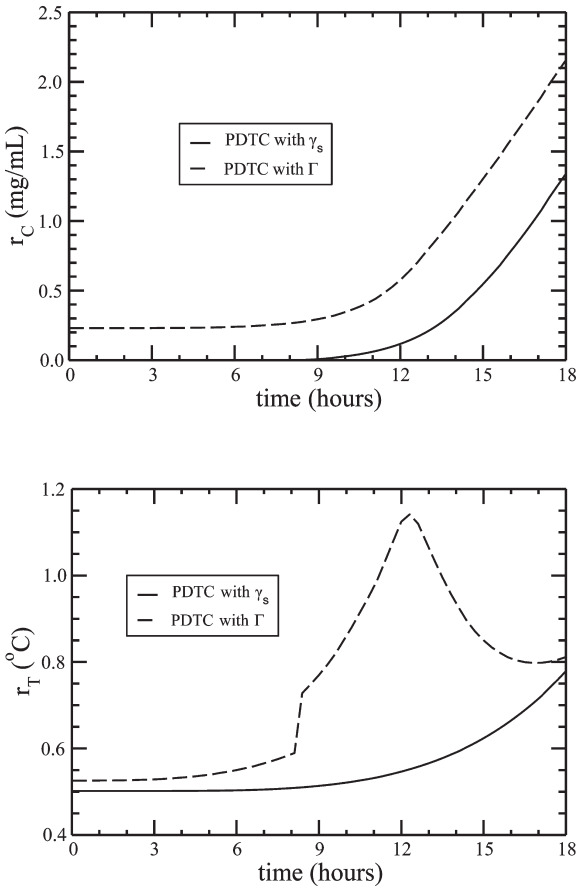

Figure 6. Comparison of the residual profiles of the protein solute concentration (r_C) and of the crystallizer temperature (r_T), relative to time during batch crystallization, in response to a parametric drift in the solubility equation (eq 3) under the PDTC scheme with γ_s and the PDTC scheme with Γ (i.e., $\Gamma = [\gamma_{110}, \gamma_{101}, \gamma_T, \gamma_C, \gamma_{nu}, \gamma_s]$), for a growth rate ratio set-point value of α_{set} = 0.89.

more narrow and closer to the set-point value than that under the PDTC with Γ.

Parametric Drifts in Growth Rates G_{110} and G_{101}. In this scenario, we look at simultaneous parametric drifts in the growth rates in the direction of the (110) and (101) faces by multiplying the expressions for G_{110} and G_{101} (cf. eqs 10 and 11, respectively) by factors of 0.7 and 0.77, respectively. This is a very typical parametric drift in the crystallization process, because the presence of impurities will reduce the overall crystal growth rates, inhibiting the attachment of molecules of interest to the crystal surface. Furthermore, an impurity may favor one face over the other, which could cause the growth

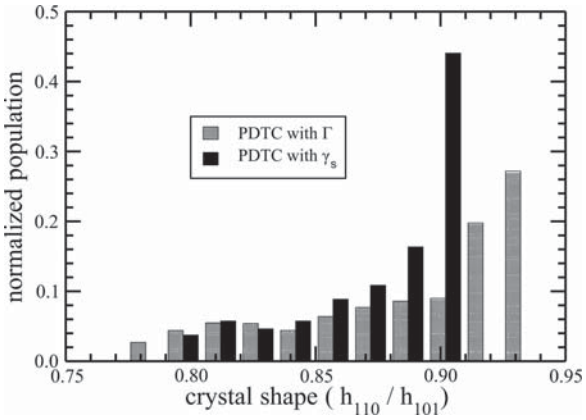

Figure 7. Normalized crystal shape distribution obtained from the kMC simulations under the PDTC scheme with γ_s is compared with that of the PDTC scheme with Γ (i.e., $\Gamma = [\gamma_{110}, \gamma_{101}, \gamma_T, \gamma_C, \gamma_{nu}, \gamma_s]$) for the batch crystallization process with a parametric drift in the solubility equation (eq 3). The desired set-point value for the average crystal shape is α_{set} = 0.89.

rate of one face to decrease more than the growth rate of the other face. When there is no PDTC implemented, as shown in Figure 8, we can observe that the values of the $r_C(t)$ and $r_T(t)$ increase progressively, because of the parametric drifts in the G_{110} and G_{101}, and eventually they exceed their thresholds, at t = 17.7 and 15.2 h, respectively. As a result, the in-batch process signature of [0;1] is obtained, indicating that there is a chance of a parametric drift in the mass balance parameters and growth rates in the direction of the (110) and (101) faces. The presence of a parametric drift is also apparent in Table 8, because the residuals $r_{\langle\alpha\rangle}(t)$, $r_{\langle h_{110}\rangle}(t)$, and $r_{\langle h_{101}\rangle}(t)$ have exceeded their thresholds at t = 18 h.

Then, we solve eq 16 to determine the magnitude of which one among the remaining three candidates better matches the in-batch and post-batch measurements. Specifically, we used both γ_{110} and γ_{101} at the same time, because it is very common in practice that growth rates in the direction of more than one face are affected by, for example, impurities. The proposed PDTC scheme then is applied to the next batch run to address the persistent parametric drifts in the G_{110} and G_{101}, where its control performance is shown in Figure 9 and Table 9, indicating that all residuals remain far below their threshold values. The performance of the parameter estimation becomes noticeable when the residuals in Tables 8 and 9 are compared. Similar to the previous case, a comparative study between the PDTC with γ_{110} and γ_{101} and the PDTC with Γ is made and shown in Figure 10 and Table 9, where the former outperforms the latter in handling the effect of the parametric drifts in the G_{110} and G_{101} parameters. This is because the PDTC with Γ may have degenerate solutions due to a limited access to the crystal product quality. As a result, it is shown in Figure 11 that crystals produced under the PDTC with γ_{110} and γ_{101} are much closer to the desired crystal shape set-point value than that under the PDTC with Γ.

Also, because of the persistent parametric drift and the nature of the batch crystallization process, it is often the case that the original set-point value is not accessible anymore and the MPC system attempts to regulate the system as close as possible to the original set-point value. For example, if G_{101} is increased by 15% (i.e., the growth rate curve for the G_{101} has shifted along the arrow in Figure 12), the optimal supersaturation level

DOI: 10.1021/acs.iecr.5b00422
Ind. Eng. Chem. Res. 2015, 54, 5514−5526

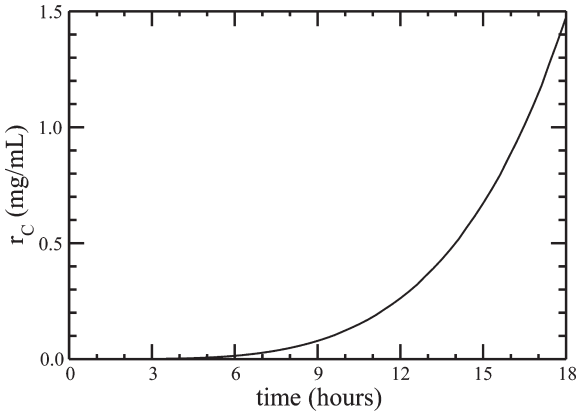

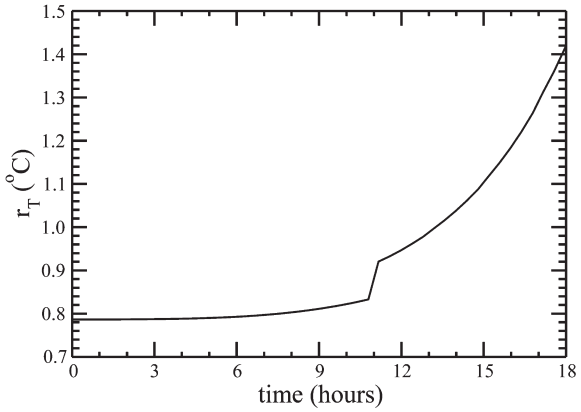

Figure 8. Residual profiles of the protein solute concentration (r_C) and of the crystallizer temperature (r_T), relative to time during batch crystallization, in response to parametric drifts in the crystal growth rates in the direction of the (110) and (101) faces (eqs 10 and 11, respectively) under the MPC scheme with the nominal process model, for a growth rate ratio set-point value of α_{set} = 0.89.

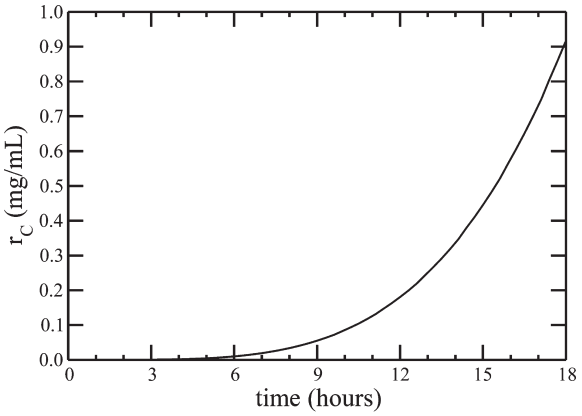

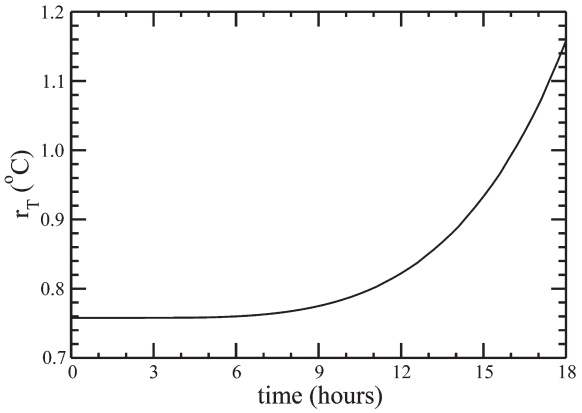

Figure 9. Comparison of the residual profiles of the protein solute concentration (r_C) and of the crystallizer temperature (r_T), relative to time during batch crystallization, in response to parametric drifts in the growth rates in the direction of the (110) and (101) faces (eqs 10 and 11, respectively) under the PDTC scheme with γ_{110} and γ_{101}, for a growth rate ratio set-point value of α_{set} = 0.89.

Table 8. Residuals Based on the Post-Batch Measurements Obtained at t = 18 h for the Batch Crystallization Process with Parametric Drifts in the Growth Rates in the Direction of the (110) and (101) Faces under No PDTC

parameter	value
$r_{\langle\alpha\rangle}$	0.088
r_{M_0}	96000
$r_{\langle h_{110}\rangle}$	21.1 μm
$r_{\langle h_{101}\rangle}$	16.6 μm

Table 9. Comparison of the Residuals Based on the Post-Batch Measurements for the Batch Crystallization Process with a Parametric Drift in the Growth Rates in the Direction of the (110) and (101) Faces under a PDTC Scheme with γ_{110} and γ_{101} and a PDTC Scheme with Γ at t = 18 h

	Value	
parameter	PDTC with γ_{110}, γ_{101}	PDTC with Γ
$r_{\langle\alpha\rangle}$	0.0088	0.028
r_{M_0}	32000	40800
$r_{\langle h_{110}\rangle}$	2.21 μm	6.28 μm
$r_{\langle h_{101}\rangle}$	2.65 μm	9.45 μm

required to achieve the set-point value (α_{set} = 0.89) is also increased, resulting in more rapid crystal growth and, as a result, more significant depletion in the protein solute concentration. As shown in Figure 13, the concentration may decrease to the level where it cannot be compensated by additionally reducing the jacket temperature, because of the constraint on the temperature of the crystallizer (cf. eq 14c). Therefore, the production of crystals with an undesirably low aspect ratio is achieved in Figure 14.

The proposed PDDI scheme can be applicable to other batch crystallization systems provided that both in-batch and post-batch measurements are available. More measurements would enhance the performance of the proposed PDDI scheme. Furthermore, in the case in which a first-principles model is not available for MPC design, the proposed PDDI scheme can be coupled with a model used in MPC that is derived from process data (i.e., a data-based model), using system identification techniques.

CONCLUSIONS

In this work, a parametric drift detection and isolation (PDDI) scheme that consists of a preparatory stage before batch-to-batch operation and a post-batch stage during batch-to-batch operation was proposed for the detection and isolation of

DOI: 10.1021/acs.iecr.5b00422
Ind. Eng. Chem. Res. 2015, 54, 5514−5526

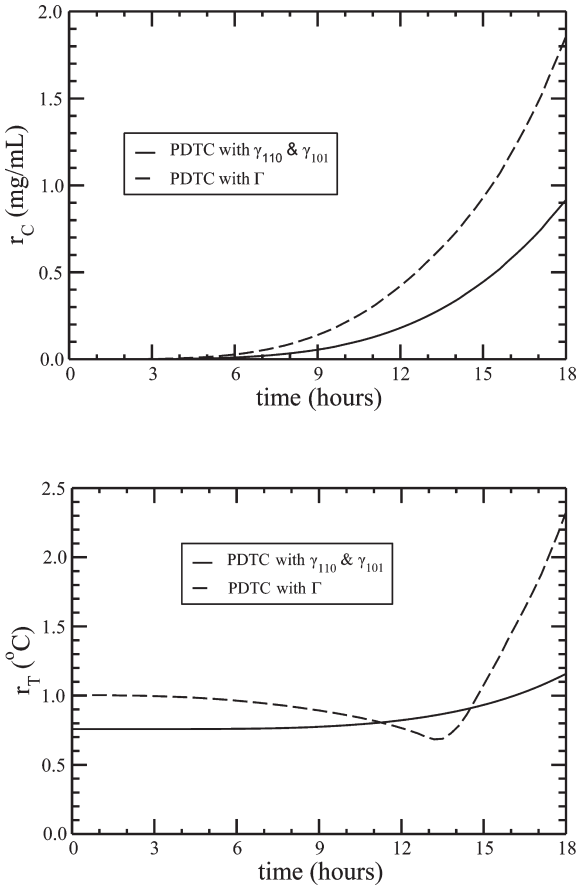

Figure 10. Comparison of the residual profiles of the protein solute concentration (r_C) and of the crystallizer temperature (r_T), relative to time during batch crystallization, in response to parametric drifts in the growth rates in the direction of the (110) and (101) faces (eqs 10 and 11, respectively) under a PDTC scheme with γ_{110} and γ_{101} and a PDTC scheme with Γ (i.e., $\Gamma = [\gamma_{110}, \gamma_{101}, \gamma_T, \gamma_C, \gamma_{nu}, \gamma_s]$), for a growth rate ratio set-point value of $\alpha_{set} = 0.89$.

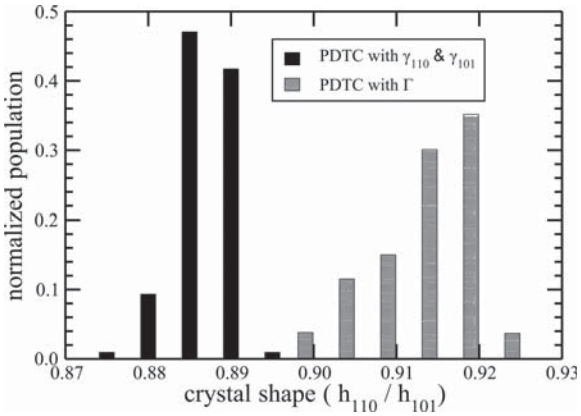

Figure 11. Normalized crystal shape distribution obtained from the kMC simulations under the PDTC scheme with γ_{110} and γ_{101}, compared with that of the PDTC scheme with Γ (i.e., $\Gamma = [\gamma_{110}, \gamma_{101}, \gamma_T, \gamma_C, \gamma_{nu}, \gamma_s]$) for the batch crystallization process with parametric drifts in the growth rates in the direction of the (110) and (101) faces (eqs 10 and 11, respectively). The desired set-point value for the average crystal shape is $\alpha_{set} = 0.89$.

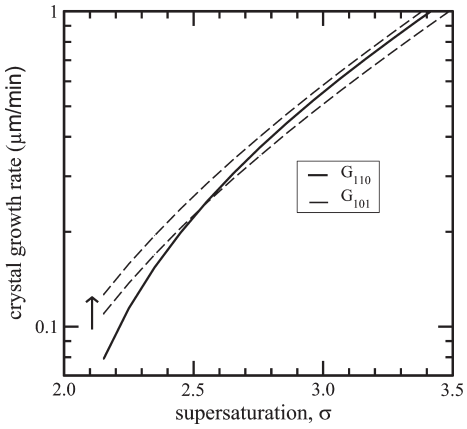

Figure 12. Solid and dashed lines show the growth rates obtained from the kMC model in the direction of the (110) and (101) faces, respectively, which are calibrated with the experimental data at 4% NaCl and pH 4.6 (taken from ref 35). The arrow indicates that the growth rate in the direction of the (101) face is increased by 15%.

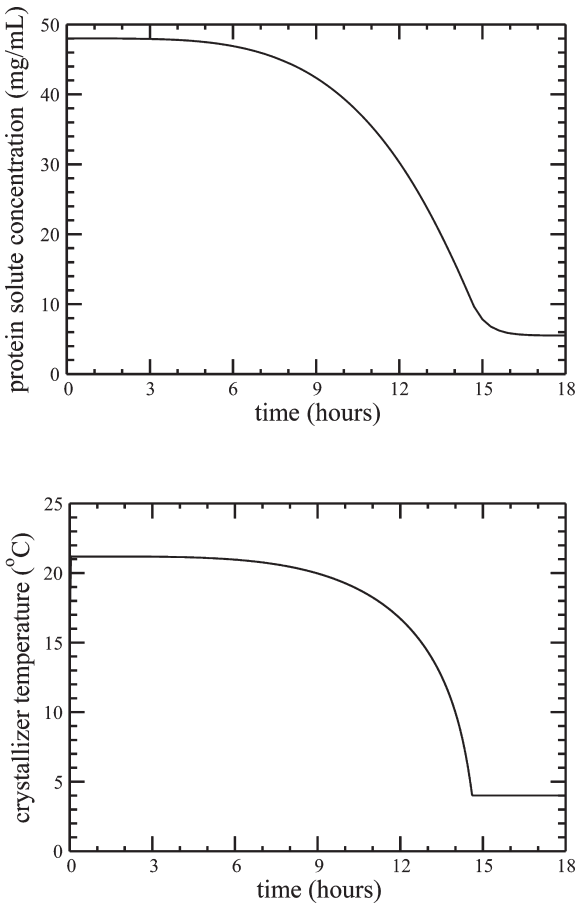

Figure 13. Comparison of the profiles of the protein solute concentration and of the crystallizer temperature with time during batch crystallization, in response to a parametric drift in the growth rate in the direction of the (101) face (eqs 10 and 11), under the PDTC scheme with γ_{101} for a growth rate ratio set-point value of $\alpha_{set} = 0.89$.

batch-to-batch parametric drifts in a batch crystallization process. In the preparatory stage, the threshold values and signatures for each parametric drift are computed without

DOI: 10.1021/acs.iecr.5b00422
Ind. Eng. Chem. Res. 2015, 54, 5514−5526

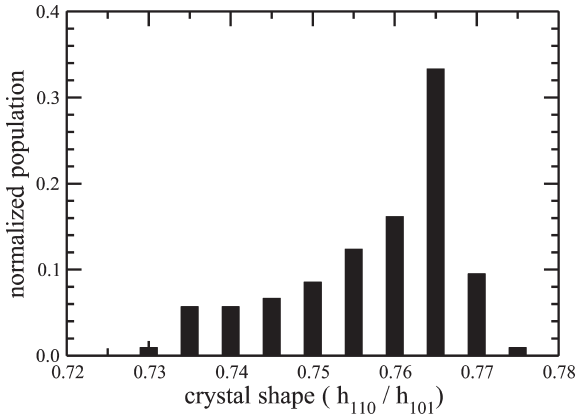

Figure 14. Normalized crystal shape distribution obtained from the kMC simulations under the PDTC scheme with γ_{101} for the batch crystallization process with a parametric drift in the growth rate in the direction of the (101) face (eqs 10 and 11). The desired set-point value for the average crystal shape is α_{set} = 0.89.

process measurements. Then, during the batch-to-batch operation, this scheme computes residuals by evaluating the absolute value of the difference between the process variables obtained from the drift-free simulation with noise from the time profiles of the states obtained through post-batch (e.g., number of crystals, average crystal size and shape) as well as in-batch (e.g., protein solute concentration, temperature in the crystallizer) process measurements. The residuals were compared with thresholds and signatures obtained in the preparatory stage for the detection and isolation of a parametric drift. Subsequently, the magnitude of the batch-to-batch parametric drift is estimated by the PDDI system and it is used to update the parameters of the batch process model which is used in the in-batch model predictive control (MPC) to compute a set of optimal jacket temperatures for the production of crystals with a desired shape distribution in the next batch. Using closed-loop simulations, the batch-to-batch process model parameter variation in the solubility and crystal growth rates were properly handled by the proposed parametric drift-tolerant control (PDTC) scheme and, as a result, the production of crystals with a desired shape distribution that is closer to a desired set-point value was achieved, compared to that of the MPC with the nominal process model. Furthermore, the performance of the proposed PDTC was evaluated, with respect to the number of correction parameters used to estimate various parametric drifts.

AUTHOR INFORMATION

Corresponding Author

*E-mail: pdc@seas.ucla.edu.

Notes

The authors declare no competing financial interest.

ACKNOWLEDGMENTS

The authors gratefully acknowledge the financial support from the Extreme Science and Engineering Discovery Environment (No. TG-CCR120003), the National Science Foundation (No. CBET-0967291), and the NSF Graduate Research Fellowship (No. DGE-1144087) given to M.N.

REFERENCES

(1) Miller, S. M.; Rawlings, J. B. Model Identification and Control Strategies for Batch Cooling Crystallizers. *AIChE J.* **1994**, *40*, 1312−1327.

(2) Worlitschek, J.; Mazzotti, M. Model-Based Optimization of Particle Size Distribution in Batch-Cooling Crystallization of Paracetamol. *Cryst. Growth Des.* **2004**, *4*, 891−903.

(3) Shi, D.; Mhaskar, P.; El-Farra, N. H.; Christofides, P. D. Predictive control of crystal size distribution in protein crystallization. *Nanotechnology* **2005**, *16*, S562−S574.

(4) Mesbah, A.; Landlust, J.; Huesman, A.; Kramer, H.; Jansens, P.; Van den Hof, P. A model-based control framework for industrial batch crystallization processes. *Chem. Eng. Res. Des.* **2010**, *88*, 1223−1233.

(5) Kalbasenka, A.; Spierings, L.; Huesman, A.; Kramer, H. Application of seeding as a process actuator in a model predictive control framework for fed-batch crystallization of ammonium sulphate. *Part. Part. Syst. Charact.* **2007**, *24*, 40−48.

(6) Kwon, J. S.; Nayhouse, M.; Christofides, P. D.; Orkoulas, G. Modeling and control of protein crystal shape and size in batch crystallization. *AIChE J.* **2013**, *59*, 2317−2327.

(7) Kwon, J. S.; Nayhouse, M.; Christofides, P. D.; Orkoulas, G. Modeling and control of crystal shape in continuous protein crystallization. *Chem. Eng. Sci.* **2014**, *107*, 47−57.

(8) Kwon, J. S.; Nayhouse, M.; Orkoulas, G.; Christofides, P. D. Enhancing crystal production rate and reducing polydispersity in continuous protein crystallization. *Ind. Eng. Chem. Res.* **2014**, *53*, 15538−15548.

(9) Bard, Y. *Nonlinear Parameter Estimation*; Academic Press: New York, 1974.

(10) Beck, J. V.; Arnold, K. J. *Parameter Estimation in Engineering and Science*; Wiley: New York, 1977.

(11) Scholl, J.; Bonalumi, D.; Vicum, L.; Mazzotti, M. *In situ* monitoring and modeling of the solvent-mediated polymorphic transformation of L-Glutamic acid. *Cryst. Growth Des.* **2006**, *6*, 881−891.

(12) Yan, W.; Shao, H.; Wang, X. Soft sensing modeling based on support vector machine and Bayesian model selection. *Comput. Chem. Eng.* **2004**, *28*, 1489−1498.

(13) Coleman, M. C.; Block, D. E. Bayesian parameter estimation with informative priors for nonlinear systems. *AIChE J.* **2006**, *52*, 651−667.

(14) Wang, J.; He, P. A bayesian approach for disturbance detection and classification and its application to state estimation in run-to-run control. *IEEE Trans. Semicond. Manuf.* **2007**, *20*, 126−136.

(15) Su, Q.; Chiu, M.; Braatz, R. D. Modeling and bayesian parmater estimation for semibatch pH-shift reactive crystallization of L-glutamic acid. *AIChE J.* **2014**, *60*, 2828−2838.

(16) Campbell, W.; Firth, S.; Toprac, A.; Edgar, T. F. A comparison of run-to-run control algorithms. *Proc. Am. Control Conf.* **2002**, 2150−2155.

(17) Su, C.; Hsu, C. A time-varying weights tuning method of the double EWMA controller. *Omega Int. J. Mange.. Sci.* **2004**, *32*, 473−480.

(18) Tseng, S.; Hsu, N. Sample-size determination for achieving asymptotic stability of a double EWMA control scheme. *IEEE Trans. Semicond. Manuf.* **2005**, *18*, 104−111.

(19) Wang, Y.; Gao, F.; Doyle, F. J. Survey on iterative learning control, repetitive control, and run-to-run control. *J. Process Control* **2009**, *19*, 1589−1600.

(20) Good, R.; Qin, S. J. Performance synthesis of multiple input multiple output (MIMO) exponentially weighted moving average (EWMA) run-to-run controller with metrology delay. *Ind. Eng. Chem. Res.* **2011**, *50*, 1400−1409.

(21) Kwon, J. S.; Nayhouse, M.; Orkoulas, G.; Ni, D.; Christofides, P. D. A method for handling batch-to-batch parametric drift using moving horizon estimation: application to run-to-run MPC of batch crystallization. *Chem. Eng. Sci.* **2015**, *127*, 210−219.

DOI: 10.1021/acs.iecr.5b00422
Ind. Eng. Chem. Res. 2015, 54, 5514−5526

(22) De Persis, C.; Isidori, A. A geometric approach to nonlinear fault detection and isolation. *IEEE Trans. Autom. Control* **2001**, *46*, 853−865.
(23) Mhaskar, P.; Gani, N. H.; El-Farra, A.; Christofides, P. D.; Davis, J. F. Integrated fault-detection and fault-tolerant control of process systems. *AIChE J.* **2006**, *52*, 2129−2148.
(24) Mhaskar, P.; McFall, C.; Gani, A.; Christofides, P. D.; Davis, J. F. Isolation and handling of actuator faults in nonlinear systems. *Automatica* **2008**, *44*, 53−62.
(25) Aradhye, H. B.; Bakshi, B. R.; Davis, J. F.; Shalt, S. C. Clustering in wavelet domain: A multiresolution ART network-based diagnostic approach. *AIChE J.* **2004**, *50*, 2455−2466.
(26) Zhang, X. D.; Parisini, T.; Polycarpou, M. M. Adaptive fault-tolerant control of nonlinear uncertain systems: an information-based diagnostic approach. *IEEE Trans. Autom. Control* **2004**, *49*, 1259−1274.
(27) Ohran, B.; Muñoz de la Peña, D.; Christofides, P. D.; Davis, J. F. Enhancing data-based fault isolation through nonlinear control. *AIChE J.* **2008**, *53*, 2734−2741.
(28) Barrett, P.; Glennon, B. Characterizing the metastable zone width and solubility curve using lasentec FBRM and PVM. *Chem. Eng. Res. Des.* **2002**, *80*, 799−805.
(29) Kougoulos, E.; Jones, A.; Jennings, K.; Wood-Kaczmar, M. Use of focused beam reflectance measurement (FBRM) and process video imaging (PVI) in a modified mixed suspension mixed product removal (MSMPR) cooling crystallizer. *J. Cryst. Growth* **2005**, *273*, 529−534.
(30) Dunuwila, D. D.; Carroll, L. B.; Berglund, K. A. An investigation of the applicability of attenuated total-reflection infrared-spectroscopy for measurement of solubility and supersaturation of aqueous citric acid solutions. *J. Cryst. Growth* **1994**, *137*, 561−588.
(31) Togkalidou, T.; Fujiwara, M.; Patel, S.; Braatz, R. Solute concentration prediction using chemometrics and ATR-FTIR spectroscopy. *J. Cryst. Growth* **2001**, *231*, 534−543.
(32) Galkin, O.; Vekilov, P. G. Nulceation of protein crystals: Critical nuclei, phase behavior, and control pathways. *J. Cryst. Growth* **2001**, *232*, 63−76.
(33) Cacioppo, E.; Pusey, M. L. The solubility of the tetragonal form of hen-egg-white lysozyme from pH 4.0 to 5.4. *J. Cryst. Growth* **1991**, *114*, 286−292.
(34) Durbin, S. D.; Feher, G. Simulation of lysozyme crystal growth by the Monte Carlo method. *J. Cryst. Growth* **1991**, *110*, 41−51.
(35) Durbin, S. D.; Feher, G. Crystal growth studies of lysozyme as a model for protein crystallization. *J. Cryst. Growth* **1986**, *76*, 583−592.
(36) Nayhouse, M.; Kwon, J. S.; Christofides, P. D.; Orkoulas, G. Crystal Shape Modeling and Control in Protein Crystal Growth. *Chem. Eng. Sci.* **2013**, *87*, 216−223.
(37) Randolph, A.; Larson, M. *Theory of Particulate Processes: Analysis and Techniques of Continuous Crystallization*; Academic Press: New York, 1988.
(38) Schall, C.; Arnold, E.; Wiencek, J. Enthalpy of crystallization of hen egg-white lysozyme. *J. Cryst. Growth* **1996**, *165*, 293−298.
(39) Hulburt, H. M.; Katz, S. Some problems in particle technology. A statistical mechanical formulation. *Chem. Eng. Sci.* **1964**, *19*, 555−574.
(40) Kwon, J. S.; Nayhouse, M.; Orkoulas, G.; Christofides, P. D. Crystal shape and size control using a plug flow crystallization configuration. *Chem. Eng. Sci.* **2014**, *119*, 30−39.

DOI: 10.1021/acs.iecr.5b00422
Ind. Eng. Chem. Res. 2015, 54, 5514−5526